We are very grateful for the reviewers' comments. A point-to-point response to reviewers' comments is provided below, and the manuscript has been revised accordingly. The line numbers in the response refer to those in the revised R1 version of the manuscript.

Response to Reviewer #1:

Comment 1: As shown in Equation 12, number size distribution of the BC cores was estimated based on the particle size distribution derived from the SMPS and the volume fraction of BC. The underlying assumption is that all the observed particles were BC containing, which is obviously wrong.

Response:

The reviewer raised an important point. In the atmosphere, not all particles may contain BC (Liu et al., 2013; Cheung et al., 2016). It has been suggested that a significant fraction of smaller size particles is non BC-containing (Cheung et al., 2016; Ma et al., 2017). BC and non-BC materials can also be externally or internally mixed. Although size resolved BC measurements were not available during this work, we have conducted size resolved Volatility Tandem Differential Mobility Analyzer (V-TDMA) measurements at 300℃ for 40, 80, 110, 150, 200 and 300 nm, respectively, during an earlier field campaign (February 2014) at the same site as in this work. At 300℃, all non-BC particle will be completely vaporized (CV) and thus the portion of non BC particles at such size, denoted as $\Phi_{N,CV}$, can be determined. The average $\Phi_{N,CV}$ values were 0.384, 0.181, 0.180, 0.158, 0.143 and 0.137, corresponding to 40, 80, 110, 150, 200 and 300 nm, respectively (Cheung et al., 2016). For particle size larger than 300 nm and less than 40 nm, $\Phi_{N,CV}$ values were set to 0.137 and 0.384, respectively. Accordingly, the complete distribution of $\Phi_{N,CV}$ for the whole PNSD was obtained. The mixing states of BC particles were also estimated here, i.e., the mass portion of externally mixed BC with respect to total BC, denoted as r_{ext}. The value of r_{ext} was taken as 0.58, which was obtained using an optical closure method during a previous field experiment at this site (Tan et al., 2016). During the following Mie theory calculation, a fixed refractive index ($\widetilde{m}_{core}$=1.80-0.54i, $\widetilde{m}_{non}$=1.55-10^{-7}i) was adopted for the whole size range. Accordingly, the calculated BC absorption at 880 nm (Abs$_{880}$) was 21.869 Mm^{-1}, which is reasonably close to the measured mean value of 21.199 Mm^{-1}. To further validate our calculation scheme (Base Case), we have considered several extreme cases. Case 1: BC is completely externally mixed with non-BC particles, i.e., $\Phi_{N,CV}$ = 0 and r_{ext} = 1; Case 2: BC is present in every size bin and BC is completely internally mixed with non-BC material, i.e., $\Phi_{N,CV}$ = 0 and r_{ext} = 0; Case 3: BC is both internally and externally mixed but there is no non BC-containing particles, i.e., $\Phi_{N,CV}$ = 0 and r_{ext} = 0.58; Case 4: BC is internally mixed with non-BC material and there is non-BC particles present, i.e., $\Phi_{N,CV}$ ranges from 0.384 to 0.137 and r_{ext} = 0; Case 5: the same as case 4 except assuming a fixed non-BC to BC ratio of 0.5, i.e., $\Phi_{N,CV}$ = 0.5, r_{ext} = 0; Case 6: the same as case 5 except that some externally mixed BC is also present, i.e., $\Phi_{N,CV}$ = 0.5, r_{ext} = 0.58. The calculation results are listed into **Table 1**. Evidently, case 1 (complete externally mixed) will significantly underestimate the measured Abs$_{880}$, indicating that most BC particles were not likely externally mixed at the Panyu site. Complete internal mixing state (case 2, 4, and 5), on the contrary, would substantially overestimate the BC absorption regardless the form of BC core distribution function. However, when the non-BC to BC ratios were considered (case base, 3, and 6), the

calculated Abs_{880} values were all very close to the measured value, showing little sensitivity to the variation in the distribution function of the BC core.

Table 1. Inter-comparison of the performance of various Mie-calculation schemes. The base case is based on the empirical distribution function and mixing states of BC particles obtained from previous field measurements at the same site. $\Phi_{N,CV}$ denotes the portion of non-BC particles and r_{ext} is the mass portion of externally mixed BC with respect to total BC. AAE_{BC} is the absorption Ångström exponent of BC, and the subscript represents the wavelength range. $Abs_{BrC,370}\%$ and $Abs_{BrC,520}\%$ are the BrC absorption contributions at 370 nm and 520 nm, respectively. $Calcabs_{880}$ is the calculated absorption at 880 nm using Mie model. $Measabs_{880}$ is the measured absorption by an Aethalometer at 880 nm. b is the intercept of the regression analysis between $Measabs_{880}$ and $Calcabs_{880}$, i.e., $Calcabs_{880}=b*\ Measabs_{880}$. R^2 is the correlation coefficient of the equation.

Case #	Scheme	$\Phi_{N,CV}$	r_{ext}	AAE $_{BC,370\text{-}520}$	AAE $_{BC,520\text{-}880}$	Abs $_{BrC,370}\%$	Abs $_{BrC,520}\%$	Calc abs$_{880}$	Meas abs$_{880}$	b	R^2
Base		0.384 to 0.137	0.58	0.723	0.962	34.13%	15.96%	21.869		1.019	0.979
1		0	1	0.331	0.626	51.64%	29.57%	15.832		0.747	0.968
2		0	0	0.856	1.128	24.76%	8.28%	27.827		1.295	0.976
3		0	0.58	0.745	0.974	33.22%	15.46%	21.936	**21.199**	1.029	0.979
4		0.384 to 0.137	0	0.835	1.111	26.01%	9.14%	27.302		1.269	0.975
5		0.5	0	0.778	1.043	29.96%	12.30%	24.921		1.150	0.968
6		0.5	0.58	0.674	0.928	36.39%	17.49%	20.897		0.977	0.975

Accordingly, the original Eq. 12 has been replaced with the following equations:

$$N(logD_p)_{CV} = N(logD_p)_{measure} \cdot \Phi(D_p)_{N,CV} \tag{12}$$

$$N(logD_p)_{BC} = N(logD_p)_{measure} \cdot (1 - \Phi(D_p)_{N,CV}) \tag{13}$$

$$r_{ext} = \frac{M_{ext}}{M_{BC}} \tag{14}$$

$$N(logD_p)_{ext} = N(logD_p)_{BC} \cdot f_{BC} \cdot r_{ext} \tag{15}$$

$$N(logD_p)_{core-shell} = N(logD_p)_{BC} \cdot (1 - f_{BC} \cdot r_{ext}) \tag{16}$$

to represent the real atmospheric BC size distributions and mixing states. In the manuscript (Line **257**), we have also inserted the following statement:

"In a realistic atmosphere, some nonlight-absorbing particles may exist independently without BC (Liu et al., 2013; Cheung et al., 2016). In this work, the portion of nonlight-absorbing particles at a certain size (D_p) was determined by our previous measurements at the same site using a Volatility Tandem Differential Mobility Analyzer (V-TDMA), during which completely vaporized (CV) particles at 300°C were referred to as nonlight-absorbing particles that externally mixed with other BC-containing particles. Thus, the PNSD of CV particles

($N(logD_p)_{CV}$) and BC-containing particles ($N(logD_p)_{CV}$) can be given by the following equations:

$$N(logD_p)_{CV} = N(logD_p)_{measure} \cdot \Phi(D_p)_{N,CV} \tag{12}$$

$$N(logD_p)_{BC} = N(logD_p)_{measure} \cdot (1 - \Phi(D_p)_{N,CV}) \tag{13}$$

where $N(logD_p)_{measure}$ is the PNSD of the measured particles from SMPS and APS.

$\Phi(D_p)_{N,CV}$ was the number fraction of CV particles.

A previous study applied three kinds of BC mixture models to calculate the aerosol optical properties, including external, homogenously internal and core-shell mixtures (Seinfeld and Pandis, 1998; Bohren and Huffman, 2007). To quantify the mixing state of BC, r_{ext} was defined as the mass fraction of externally mixed BC (M_{ext}) in total BC (M_{BC}):

$$r_{ext} = \frac{M_{ext}}{M_{BC}} \tag{14}$$

Tan et al. (2016) suggested that two extreme conditions of external and core-shell mixtures comprised the actual mixing state of BC in the PRD. Hence, we simply divided the PNSD of BC into the PNSD from an external mixture of BC and a core-shell mixture of BC. The PNSDs of externally mixed BC particles and core-shell mixed BC particles were referred to by the following equations with a given r_{ext}.

$$N(logD_p)_{ext} = N(logD_p)_{BC} \cdot f_{BC} \cdot r_{ext} \tag{15}$$

$$N(logD_p)_{core-shell} = N(logD_p)_{BC} \cdot (1 - f_{BC} \cdot r_{ext}) \tag{16}$$

f_{BC} was defined as the BC volume fraction in the total particle volume, which can be converted from the BC mass concentration:

$$f_{BC} = \frac{M_{BC}}{\rho_{BC} \cdot \Sigma_{D_P} N(logD_p)_{BC} \cdot (\frac{\pi}{6} \cdot D_p^3)} \tag{17}$$

where ρ_{BC} is the density of BC and is assumed to be 1.5 g cm^{-3} (Ma et al., 2012); M_{BC} is the BC mass concentration derived from the multi-angle absorption photometer (MAAP), which was obtained by an empirical formula from the Aethalometer that measured the BC concentration ($M_{BC,AE}$), as proposed by Wu et al. (2009):

$$M_{BC} = 0.897 \cdot M_{BC,AE} - 0.062 \tag{18}$$

The PNSDs of externally mixed nonlight-absorbing particles and externally mixed BC particles were input into the BHMIE code, and the PNSD of the core-shell mixed particles was imported into the BHCOAT code. Another critical parameter for the core-shell model was the diameter of the BC core. For the simplified core-shell model we applied, the visualization was that a homogeneous BC core sphere was encapsulated in a shell of non-absorbing coating (Bohren and Huffman, 2007). Without size-resolved coating thickness measurements, core-shell mixed particles simply assumed that cores with the same diameter had the same coating thickness. Therefore, the diameter of the BC core was calculated as follows:

$$D_{core} = D_p \cdot (\frac{f_{BC} - f_{BC} \cdot r_{ext}}{1 - f_{BC} \cdot r_{ext}})^{\frac{1}{3}} \tag{19}$$

D_{core} and D_p are inputted as parameters into a_n and b_n, respectively, which was described by Bohren and Huffman (2007). Thus, the $\sigma_{abs,BC,Mie,\lambda_i}$ values of all six wavelengths were calculated through the Mie model, and then the AAE_{BC} values of those five wavelengths were obtained using Eq. (6). The performance of this empirically determined calculation method has

been compared with other possible BC mixing schemes in details (see Table 1)."

In addition, using the new Eqs. 12-16 and under the assumption of unit AAE_{BC}, the campaign-averaged σ_{BrC} values were 17.6±13.7 Mm^{-1} at 370 nm, 9.7±7.9 Mm^{-1} at 470 nm, 5.8±5.1 Mm^{-1} at 520 nm, 4.0±3.5 Mm^{-1} at 590 nm and 2.3±2.1 Mm^{-1} at 660 nm. At the corresponding wavelengths, BrC absorption contributed 26.2±8.5%, 20.0±7.3%, 14.3±6.5%, 11.7±5.3%, and 7.8±4.1% to the total aerosol absorption, respectively. When the AAE_{BC} was applied as the result of the Mie model calculation, the corrected campaign-averaged $\sigma_{abs,BrC}$ values were 23.5±17.7 Mm^{-1} at 370 nm, 11.8±9.5 Mm^{-1} at 470 nm, 6.7±5.7 Mm^{-1} at 520 nm, 4.6±3.9 Mm^{-1} at 590 nm and 2.6±2.3 Mm^{-1} at 660 nm. At the corresponding wavelengths, BrC absorption contributed 34.1±8.0%, 23.7±7.3%, 16.0±6.7%, 13.0±5.4%, and 8.7±4.3% to the total aerosol absorption (see Fig. 2), respectively. This statement has been inserted into the manuscript in Line **373**.
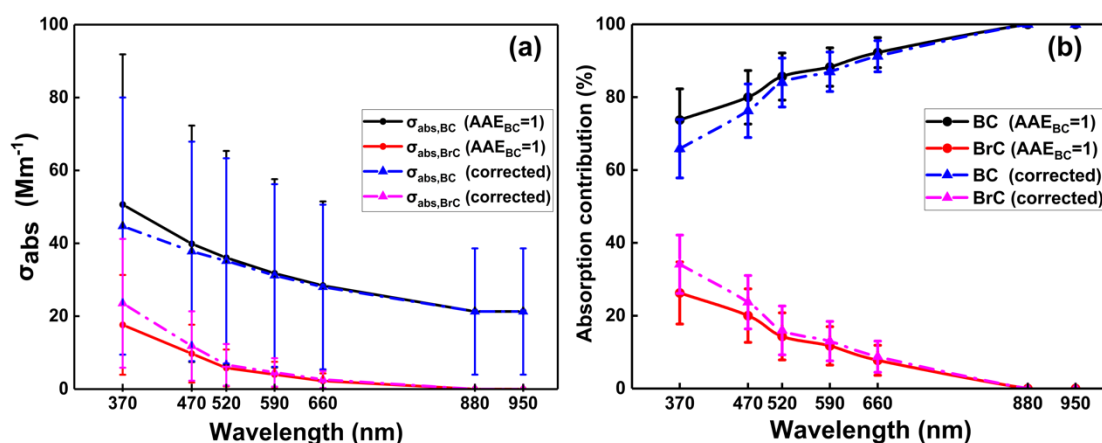
Figure 2. (a) BC and BrC particle average light absorption coefficients at different wavelengths under different AAE_{BC} assumptions; the whiskers represent an error of one standard deviation. (b) Contributions of BC and BrC to the total light absorption coefficient at different wavelengths under different AAE_{BC} assumptions; the whiskers represent an error of one standard deviation.

Comment 2: *As shown in Eq. 13, the volume fraction of BC is determined based on the "volume" of BC (V1) and the "volume" of whole particles (V2). V1 is calculated as the ratio of BC mass to the material density of BC, indicating V1 is related to the mass-equivalent size. However, V2 is based on the mobility size. I think it is not proper to calculate the BC volume fraction simply as the ratio of V1 to V2.*

Response:
We appreciate the reviewer's comment. In the simplified Mie model, the BC core was assumed as homogeneous sphere and its mass was determined with the material density of BC. Therefore, the V1 should be mass-equivalent after being normalized by the BC material density. Furthermore, for spherical particles, electrical mobility diameter (D_m) equals its physical diameter (D_p) and volume equivalent diameter (D_{ve}) as suggested by DeCarlo et al. (2004).

In the manuscript, we have revised the statement as (Line **274**):

"Tan et al. (2016) suggested that two extreme conditions of external and core-shell mixtures comprised the actual mixing state of BC in the PRD. Hence, we simply divided the PNSD of BC into the PNSD from an external mixture of BC and a core-shell mixture of BC. The PNSDs of externally mixed BC particles and core-shell mixed BC particles were referred to by the following equations with a given r_{ext}.

$$N(logD_p)_{ext} = N(logD_p)_{BC} \cdot f_{BC} \cdot r_{ext} \qquad (15)$$

$$N(logD_p)_{core-shell} = N(logD_p)_{BC} \cdot (1 - f_{BC} \cdot r_{ext}) \qquad (16)$$

f_{BC} was defined as the BC volume fraction in the total particle volume, which can be converted from the BC mass concentration:

$$f_{BC} = \frac{M_{BC}}{\rho_{BC} \cdot \Sigma_{D_P} N(logD_p)_{BC} \cdot (\frac{\pi}{6} \cdot D_p^3)} \qquad (17)$$

where ρ_{BC} is the density of BC and is assumed to be 1.5 g cm^{-3} (Ma et al., 2012); M_{BC} is the BC mass concentration derived from the multi-angle absorption photometer (MAAP), which was obtained by an empirical formula from the Aethalometer that measured the BC concentration ($M_{BC,AE}$), as proposed by Wu et al. (2009):

$$M_{BC} = 0.897 \cdot M_{BC,\,AE} - 0.062 \qquad (18)"$$

Comment 3: *Please clarify how the coating thickness is parameterized for the Mie simulations.*

Response:
As suggested by Bohren and Huffman (2007), the core-shell model is assuming a uniformly distributed spherical configuration with different parameters (Eqs. 8 and 9) for different materials. To clarify this parameterization for the Mie simulations, we have revised the expression in the manuscript as (Line **291**):

"Another critical parameter for the core-shell model was the diameter of the BC core. For the simplified core-shell model we applied, the visualization was that a homogeneous BC core sphere was encapsulated in a shell of non-absorbing coating (Bohren and Huffman, 2007). Without size-resolved coating thickness measurements, core-shell mixed particles simply assumed that cores with the same diameter had the same coating thickness. Therefore, the diameter of the BC core was calculated as follows:

$$D_{core} = D_p \cdot (\frac{f_{BC} - f_{BC} \cdot r_{ext}}{1 - f_{BC} \cdot r_{ext}})^{\frac{1}{3}} \qquad (19)$$

D_{core} and D_p are inputted as parameters into a_n and b_n, respectively, which was described by Bohren and Huffman (2007). Thus, the $\sigma_{abs,BC,Mie,\,\lambda_i}$ values of all six wavelengths were calculated through the Mie model, and then the AAE$_{BC}$ values of those five wavelengths were obtained using Eq. (6)."

Comment 4: *Abbreviations should be defined when they are used for the first time (e.g., BC in Line 48, SSA in Line 88, MAAP in Line 251). (2) Line 48-50. Please note that globally, open burning is the largest source of BC.*

Response:

As suggested by the reviewer, we have defined the abbreviations accordingly. In Line **49**, we have revised the manuscript as: "Black carbon (BC) and organic carbon (OC) are dominant carbonaceous aerosol components that mainly originate from biomass burning in a global scale (Bond et al., 2004) and have attracted great environmental concerns in rapidly developing regions."

Comment 5: *Line 66. BC absorption is wavelength-dependent. As mentioned by the authors themselves, the AAE is about 1.0 for BC.*

Response:
Yes, the reviewer is correct. Since the RI of BC is different at different wavelength, BC absorption is certainly wavelength-dependent. We have corrected the sentence as "BC absorption is commonly assumed to be covering the full wavelength-range."

Comment 6: *Line 105. It should be "seven-wavelength". (5) Please use either "Aethalometer" or "aethalometer". (6) Line 116. Please check the presentation of the longitude and latitude.*

Response:
As suggested by the reviewer, "seven-wavelengths" has been changed to "seven-wavelength" in the revised manuscript (Lines **108** and **188**). "Aethalometer" is now used throughout the manuscript. The longitude and latitude of the observation site has been inserted into the manuscript (Line **119**) "113°21′E, 23°00′N".

Comment 7: *Line 163-164. Please note that laser transmittance is monitored throughout thermal-optical analysis, rather than only for the OC stage.*

Response:
As suggested by the reviewer, we have corrected it in the revised manuscript (Line **168**):
"To correct the PC converted from OC to EC, a tunable pulsed diode laser beam was used to monitor the laser transmittance through the quartz filter throughout the thermal-optical analysis (Bauer et al., 2012)."

Comment 8: *Line 296. What does "range substantially" mean? I guess the authors may want to say "vary substantially".*

Response:
We have corrected it as (Line **385**) "vary substantially".

Comment 9: *Line 381. I can understand that for the chemical components measured in the present study, there was no better tracer than K+ for biomass burning. However, limitations of using K+ should be discussed (e.g., Aerosol and Air Quality Research, 18: 2447–2459, 2018). Maybe it is better to correct the observed K+ for sea salt and crustal materials and then use the correct K+ for discussions on biomass burning.*

Response:

We agree with the reviewer that there are other sources of K$^+$, such as sea salt and crustal materials. We have corrected the K$^+$ concentrations following the method suggested by Jung et al. (2014), using Na$^+$ as a tracer for sea salt and Ca^{2+} as a tracer for crustal materials:

Then, we tried to apply a correction method to acquire K$^+$ concentrations from biomass burning (K$_{BB}^+$) followed Jung et al. (2014), and uses Na$^+$ as a tracer for sea salt and Ca^{2+} for a tracer for crustal materials:

$$K_{BB}^+ = K^+ - [K^+/Na^+]_{seawater} \times Na^+ - [K^+/Ca^{2+}]_{crustal} \times nssCa^{2+}/(1-0.1 \times [K^+/Ca^{2+}]_{crustal}) \qquad (S1)$$

where K$_{BB}^+$ denotes K$^+$ from biomass burning; [K$^+$/Ca^{2+}]$_{crustal}$ is the emission ratio of K$^+$ from crustal materials with respect to Ca^{2+} and a value of 0.12 is used here; [K$^+$/Na$^+$]$_{seawater}$ is the mass ratio of potassium to sodium in seawater with a value of 0.036; and nssCa^{2+} represents non-sea-salt Ca^{2+} as suggested by Pio et al. (2007). A plot of the correlation between K$^+$ and K$_{BB}^+$ has been inserted into the supplementary information as Fig. S1. It is clearly shown that K$_{BB}^+$ is well correlated with K$^+$ and K$_{BB}^+$ is ~1.5% lower than measured K$^+$, indicating that the potential interferences from sea salt and crustal materials are relatively small. Earlier researches in Guangzhou also suggested that the contribution of sea salt to water soluble fraction of PM$_{2.5}$ was trivial (Lai et al., 2007) and dust-related aerosol contribution of PM$_{2.5}$ was less than 5% (Huang et al., 2014). The above discussion has been inserted into the supplement information as Fig. S1.
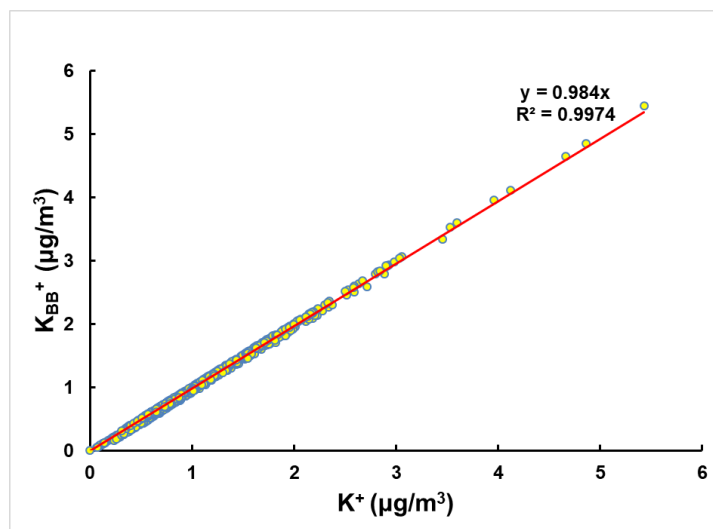
Figure S1. The correlation between the K$^+$ and K$_{BB}^+$.

However, Eq. S1 does not consider the impact of another possible K$^+$ source, such as coal combustion. It would be difficult to estimate K$^+$ emission from coal combustion without heavy metal measurements. The coal consumption in the PRD region was dominated by coal-fired power plants. The emission from power plants was usually very steady and was less likely to affect to the diurnal correlation between K$^+$ and BrC absorption. As shown in Fig. 9d, the ratios of K$^+$/PM$_{2.5}$ varies approximately between 0.015 and 0.020 and the diurnal profile of K$^+$/PM$_{2.5}$ shows very little variation. Yu et al. (2018) have suggested that K$^+$ usually accounted for 2.34-5.49% of PM$_{2.5}$ in laboratory biomass burning study. However, K$^+$ was normally lower than 1%

of coal combustion PM$_{2.5}$. Therefore, the ratio range of K$^+$ to PM$_{2.5}$ observed in this work likely indicated aged biomass burning particles.

The following statement has been inserted into the manuscript (Line **528**):

"Although the geographic location of the observation site was situated in a coastal area and K$^+$ could also be found in sea salt (Pio et al., 2008), it should be noted that the prevailing wind direction during winter was from the north (see Fig. 3), which drives maritime air parcels away from the site. Hence, the effect of sea salt and crustal materials to K$^+$ was slight, which was demonstrated in the supplementary information as shown in Fig. S1. Other earlier studies also suggested that the sea salt contribution to the water-soluble fraction of PM$_{2.5}$ was trivial in the PRD region (Lai et al., 2007). Another possible K$^+$ source was coal combustion. The coal consumption in the PRD region was dominated by coal-fired power plants. The emission from power plants was usually very steady and was less likely to affect the diurnal correlation between K$^+$ and BrC absorption. As shown in Fig. 9, the ratios of K$^+$/PM$_{2.5}$ varies approximately from 0.015 to 0.020 and the diurnal profile of K$^+$/PM$_{2.5}$ shows very little variation. Yu et al. (2018) have suggested that K$^+$ usually accounted for 2.34-5.49% of PM$_{2.5}$ in the laboratory biomass burning study. However, K$^+$ is normally lower than 1% of coal combustion PM$_{2.5}$. Therefore, the ratio range of K$^+$ to PM$_{2.5}$ observed in this work likely indicated aged biomass burning particles."
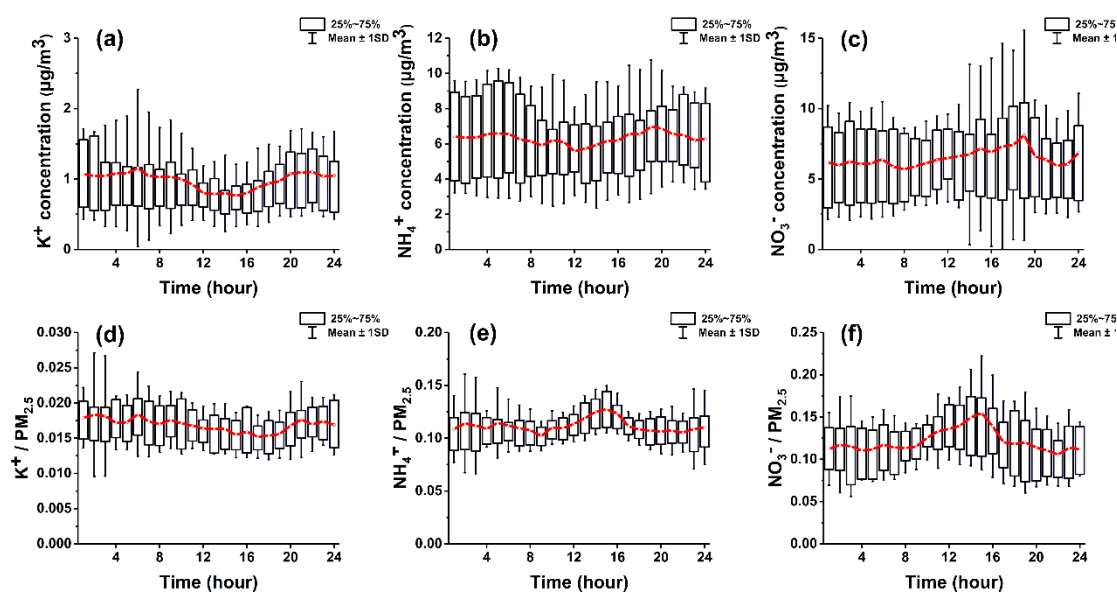
Figure 9. Box-whisker plots of diurnal trends in K$^+$ concentration (a), NH$_4^+$ concentration (b), NO$_3^-$ concentration (c), K$^+$/PM$_{2.5}$ (d), NH$_4^+$/PM$_{2.5}$ (e) and NO$_3^-$/PM$_{2.5}$ (f).

Comment 10: *Line 416-417. Please explain the absence of K+ peak during the lunch and dinner time.*

Response:

In Fig. 9, no distinct lunch and dinner peaks of K$^+$ are shown in the diurnal profile. In fact, the early morning peak of K$^+$ is also barely distinguishable, indicating that biofuel is not heavily used in the PRD region. The other possible reason is that the boundary layer height is much

higher during lunch and dinner time than in the early morning, providing a much better atmospheric diffusion condition. The statement has been revised as (Line **504**):

"Unlike OC, K^+ shows a small peak at approximately 6 AM, which was consistent with breakfast time and was very likely due to cooking activities using biofuel. No lunch and dinner time K^+ peaks were observed. The most likely explanation is that the boundary layer height is much higher during lunch and dinner time than in the early morning, providing a much better atmospheric diffusion condition for air pollutants. It is still a common practice to collect straw as biofuel in local rural areas, which can be visually spotted but is not heavily utilized in the region."

Comment 11: *Line 432-439. Although NOx and NH₃ can be found in biomass burning emissions, this does not necessarily mean that nitrate and ammonium can be used as tracers for biomass burning, i.e., the correlation between BrC and nitrate or ammonium cannot demonstrate biomass burning as an important source of BrC.*

Response:

The reviewer is correct. Nitrate and NH_3 cannot be used exclusively as biomass burning tracers. Their presence inside the biomass burning plumes can be partially explained by the photochemical processes. The statement has been revised as (Line **543**):

"For NO_3^- and NH_4^+, nitrate can be converted from NO_x through atmospheric reactions, and ammonium may originate from NH_3. However, similar to the diurnal variation in $\sigma_{abs,BrC,370nm}$, diurnal variations in NH_4^+ and NO_3^- also increased in the afternoon and appeared at nighttime in Fig 9. However, $NO_3^-/PM_{2.5}$ and $NH_4^+/PM_{2.5}$ reached their peaks at noon, indicating that ammonium nitrate formed from the secondary reaction at this time. Along with the reduced boundary layer height and ambient temperature, NO_3^- was accumulated until the photochemical reaction stopped at night. The diurnal variation in NH_4^+ was similar to that in NO_3^- due to the acid/base neutralization reaction. The overlapping of the $\sigma_{abs,BrC,370nm}$, NH_4^+ and NO_3^- diurnal variations would lead to a significant correlation between BrC absorption and NO_3^- or NH_4^+."

Reviewer #2:

Comment 1: However, the uncertainty in AAE_{BC} is replaced by a calculation in which the number size distribution of the BC core is assumed to be a scaled fraction of the overall number size distribution. Also as pointed out by the other reviewer, this seems to be a questionable assumption; in addition, the scaling factor is derived as a volume fraction - so if applied, it would be the volume size distribution that should be scaled by this number.

Response:

We appreciate the very helpful suggestion provided by the reviewer. There is a typo in the original Eq. 12, i.e., the f_{BC} term should be removed. The original Eq. 12 meant that the size distribution of the BC core was the same as the measured PNSD. We also agree with both reviewers that not all particle may contain BC and the size distribution of BC core may also vary with particle size. Therefore, we have developed an empirical formula to account for the BC distribution function and mixing states.

Although size resolved BC measurements were not available during this work, we have conducted size resolved Volatility Tandem Differential Mobility Analyzer (V-TDMA) measurements at 300℃ for 40, 80, 110, 150, 200 and 300 nm, respectively, during an earlier field campaign (February 2014) at the same site as in this work. At 300℃, all non-BC particle will be completely vaporized (CV) and thus the portion of non BC particles at such size, denoted as $\Phi_{N,CV}$, can be determined. The average $\Phi_{N,CV}$ values were 0.384, 0.181, 0.180, 0.158, 0.143 and 0.137, corresponding to 40, 80, 110, 150, 200 and 300 nm, respectively (Cheung et al., 2016). For particle size larger than 300 nm and less than 40 nm, $\Phi_{N,CV}$ values were set to 0.137 and 0.384, respectively. Accordingly, the complete distribution of $\Phi_{N,CV}$ for the whole PNSD was obtained. The mixing states of BC particles were also estimated here, i.e., the mass portion of externally mixed BC with respect to total BC, denoted as r_{ext}. The value of r_{ext} was taken as 0.58, which was obtained using an optical closure method during a previous field experiment at this site (Tan et al., 2016). During the following Mie theory calculation, a fixed refractive index ($\widetilde{m}_{core}$=1.80-0.54i, $\widetilde{m}_{non}$=1.55-10^{-7}i) was adopted for the whole size range. Accordingly, the calculated BC absorption at 880 nm (Abs_{880}) was 21.869 Mm^{-1}, which is reasonably close to the measured mean value of 21.199 Mm^{-1}. To further validate our calculation scheme (Base Case), we have considered several extreme cases. Case 1: BC is completely externally mixed with non-BC particles, i.e., $\Phi_{N,CV}$ = 0 and r_{ext} = 1; Case 2: BC is present in every size bin and BC is completely internally mixed with non-BC material, i.e., $\Phi_{N,CV}$ = 0 and r_{ext} = 0; Case 3: BC is both internally and externally mixed but there is no non BC-containing particles, i.e., $\Phi_{N,CV}$ = 0 and r_{ext} = 0.58; Case 4: BC is internally mixed with non-BC material and there is non-BC particles present, i.e., $\Phi_{N,CV}$ ranges from 0.384 to 0.137 and r_{ext} = 0; Case 5: the same as case 4 except assuming a fixed non-BC to BC ratio of 0.5, i.e., $\Phi_{N,CV}$ = 0.5, r_{ext} = 0; Case 6: the same as case 5 except that some externally mixed BC is also present, i.e., $\Phi_{N,CV}$ = 0.5, r_{ext} = 0.58. The calculation results are listed into **Table 1**. Evidently, case 1 (complete externally mixed) will significantly underestimate the measured Abs_{880}, indicating that most BC particles were not likely externally mixed at the Panyu site. Complete internal mixing state (case 2, 4, and 5), on the contrary, would substantially overestimate the BC absorption regardless the form of BC core distribution function. However, when the non-BC to BC ratios were considered (case base, 3, and 6), the calculated Abs_{880} values were all very close to the measured value,

showing little sensitivity to the variation in the distribution function of the BC core.

In the manuscript, we have revised the related statement as (Line **274**):

"Tan et al. (2016) suggested that two extreme conditions of external and core-shell mixtures comprised the actual mixing state of BC in the PRD. Hence, we simply divided the PNSD of BC into the PNSD from an external mixture of BC and a core-shell mixture of BC. The PNSDs of externally mixed BC particles and core-shell mixed BC particles were referred to by the following equations with a given r_{ext}.

$$N(logD_p)_{ext} = N(logD_p)_{BC} \cdot f_{BC} \cdot r_{ext} \tag{15}$$

$$N(logD_p)_{core-shell} = N(logD_p)_{BC} \cdot (1 - f_{BC} \cdot r_{ext}) \tag{16}$$

f_{BC} was defined as the BC volume fraction in the total particle volume, which can be converted from the BC mass concentration:

$$f_{BC} = \frac{M_{BC}}{\rho_{BC} \cdot \sum_{D_P} N(logD_p)_{BC} \cdot (\frac{\pi}{6} \cdot D_p^3)} \tag{17}$$

where ρ_{BC} is the density of BC and is assumed to be 1.5 g cm^{-3} (Ma et al., 2012); M_{BC} is the BC mass concentration derived from the multi-angle absorption photometer (MAAP), which was obtained by an empirical formula from the Aethalometer that measured the BC concentration ($M_{BC,AE}$), as proposed by Wu et al. (2009):

$$M_{BC} = 0.897 \cdot M_{BC, AE} - 0.062 \tag{18}"$$

Comment 2: *Given the large uncertainty in black carbon forcing based on actual size distribution and particle morphology (core-shell or not - e.g., Cappa et al., doi:10.1126/science.1223447, 2012), it's unclear whether the BrC forcing can be satisfactorily constrained, even with this accomplished suite of instruments, without additional information from an SP2 or chemical transport modeling simulations.*

Response:

We agree with the reviewer that the uncertainty associated with the BC climate forcing are most likely due to the complicated BC size distribution, mixing states, and morphology. The new advancement in measurement techniques, such as SP2, has provided more insight into the detailed information about atmospheric BC. Nevertheless, the core-shell model has been widely utilized to simulate the BC optical properties, especially in various atmospheric modeling studies. In fact, the BC coating thickness measured by all instruments, including SP2, are deduced using a core-shell configuration. We agree with the reviewer that a simple uniform BC core distribution will not capture the real atmospheric BC core size distribution. Therefore, we have developed an empirical formula to account for the BC size distribution and mixing states for the study area. The results (Table 1) show that the calculated BC absorption agreed fairly well (within 3%) with the observed BC absorption. In addition, we have validated the effectiveness of this formula by varying the BC size distribution function and mixing states as explained in details in our response to comment 1, which demonstrated that using a uniform BC distribution function may only lead to a small error in the calculated BC absorption and the variation of the BC mixing state will cause the most significant change in the calculated absorption value. In this study, we found most of the observed BC-containing particles were very likely originated from aged biomass burning plumes, which usually contain thickly coated BC particles. Therefore, we concluded that our empirical formula fit well into this particular

study area.

References:

Liu, D., Allan, J., Whitehead, J., Young, D., Flynn, M., Coe, H., McFiggans, G., Fleming, Z. L., and Bandy, B.: Ambient black carbon particle hygroscopic properties controlled by mixing state and composition, Atmos. Chem. Phys., 13, 2015-2029, 10.5194/acp-13-2015-2013, 2013.

Cheung, H. H. Y., Tan, H., Xu, H., Li, F., Wu, C., Yu, J. Z., and Chan, C. K.: Measurements of non-volatile aerosols with a VTDMA and their correlations with carbonaceous aerosols in Guangzhou, China, Atmos. Chem. Phys., 16, 8431-8446, 10.5194/acp-16-8431-2016, 2016.

Ma, Y., Li, S. Z., Zheng, J., Khalizov, A., Wang, X., Wang, Z., and Zhou, Y. Y.: Size-resolved measurements of mixing state and cloud-nucleating ability of aerosols in Nanjing, China, J. Geophys. Res.-Atmos., 122, 9430-9450, 10.1002/2017jd026583, 2017.

Tan, H., Liu, L., Fan, S., Li, F., Yin, Y., Cai, M., and Chan, P. W.: Aerosol optical properties and mixing state of black carbon in the Pearl River Delta, China, Atmospheric Environment, 131, 196-208, http://dx.doi.org/10.1016/j.atmosenv.2016.02.003, 2016.

Seinfeld, J. H., and Pandis, S. N.: Atmospheric Chemistry and Physics, John Wiley & Sons, Inc, New York, 1998.

Bohren, C. F., and Huffman, D. R.: Absorption and Scattering of Light by Small Particles, WILEY-VCH Verlag GmbH & Co. KGaA 328-328 pp., 2007.

Ma, N., Zhao, C. S., Müller, T., Cheng, Y. F., Liu, P. F., Deng, Z. Z., Xu, W. Y., Ran, L., Nekat, B., van Pinxteren, D., Gnauk, T., Müller, K., Herrmann, H., Yan, P., Zhou, X. J., and Wiedensohler, A.: A new method to determine the mixing state of light absorbing carbonaceous using the measured aerosol optical properties and number size distributions, Atmos. Chem. Phys., 12, 2381-2397, 10.5194/acp-12-2381-2012, 2012.

Wu, D., Mao, J., Deng, X., Tie, X., Zhang, Y., Zeng, L., Li, F., Tan, H., Bi, X., Huang, X., Chen, J., and Deng, T.: Black carbon aerosols and their radiative properties in the Pearl River Delta region, Science in China Series D: Earth Sciences, 52, 1152-1163, 10.1007/s11430-009-0115-y, 2009.

DeCarlo, P. F., Slowik, J. G., Worsnop, D. R., Davidovits, P., and Jimenez, J. L.: Particle Morphology and Density Characterization by Combined Mobility and Aerodynamic Diameter Measurements. Part 1: Theory, Aerosol Science & Technology, 38, 1185-1205, 2004.

Bond, T. C., Streets, D. G., Yarber, K. F., Nelson, S. M., Woo, J. H., and Klimont, Z.: A technology-based global inventory of black and organic carbon emissions from combustion, J. Geophys. Res.-Atmos., 109, 43, 10.1029/2003jd003697, 2004.

Bauer, J. J., Yu, X.-Y., Cary, R., Laulainen, N., and Berkowitz, C.: Characterization of the Sunset Semi-Continuous Carbon Aerosol Analyzer, Journal of the Air & Waste Management

Association, 59, 826-833, 10.3155/1047-3289.59.7.826, 2012.

Jung, J., Lee, S., Kim, H., Kim, D., Lee, H., and Oh, S.: Quantitative determination of the biomass-burning contribution to atmospheric carbonaceous aerosols in Daejeon, Korea, during the rice-harvest period, Atmospheric Environment, 89, 642-650, 10.1016/j.atmosenv.2014.03.010, 2014.

Pio, C. A., Legrand, M., Oliveira, T., Afonso, J., Santos, C., Caseiro, A., Fialho, P., Barata, F., Puxbaum, H., Sanchez-Ochoa, A., Kasper-Giebl, A., Gelencser, A., Preunkert, S., and Schock, M.: Climatology of aerosol composition (organic versus inorganic) at nonurban sites on a west-east transect across Europe, J. Geophys. Res.-Atmos., 112, 10.1029/2006jd008038, 2007.

Lai, S.-c., Zou, S.-c., Cao, J.-j., Lee, S.-c., and Ho, K.-f.: Characterizing ionic species in PM2.5 and PM10 in four Pearl River Delta cities, South China, Journal of Environmental Sciences, 19, 939-947, https://doi.org/10.1016/S1001-0742(07)60155-7, 2007.

Huang, R.-J., Zhang, Y., Bozzetti, C., Ho, K.-F., Cao, J.-J., Han, Y., Daellenbach, K. R., Slowik, J. G., Platt, S. M., Canonaco, F., Zotter, P., Wolf, R., Pieber, S. M., Bruns, E. A., Crippa, M., Ciarelli, G., Piazzalunga, A., Schwikowski, M., Abbaszade, G., Schnelle-Kreis, J., Zimmermann, R., An, Z., Szidat, S., Baltensperger, U., Haddad, I. E., and Prévôt, A. S. H.: High secondary aerosol contribution to particulate pollution during haze events in China, Nature, 514, 218-222, 10.1038/nature13774, 2014.

Yu, J., Yan, C., Liu, Y., Li, X., Zhou, T., and Zheng, M.: Potassium: A Tracer for Biomass Burning in Beijing?, Aerosol and Air Quality Research, 18, 2447-2459, 10.4209/aaqr.2017.11.0536, 2018.

Pio, C. A., Legrand, M., Alves, C. A., Oliveira, T., Afonso, J., Caseiro, A., Puxbaum, H., Sanchez-Ochoa, A., and Gelencsér, A.: Chemical composition of atmospheric aerosols during the 2003 summer intense forest fire period, Atmospheric Environment, 42, 7530-7543, 2008.